

1 **Subsidence of the West Siberian Basin: Effects of a**  
2 **mantle plume impact**

3 **Peter J. Holt**

4 **Jeroen van Hunen**

5 **Mark B. Allen**

6 *Department of Earth Sciences, Durham University, Durham, DH1 3LE, UK*

7

8 **ABSTRACT**

9 Comparison of modelling results with observed subsidence patterns from the West  
10 Siberian Basin provides new insight into the origin of the Siberian Traps, and constrains  
11 the temperature, size, and depth of an impacting mantle plume head during and after the  
12 eruption of the Siberian Traps at the Permian-Triassic boundary (250 Ma). We compare  
13 synthetic subsidence patterns from 1-D conductive heat flow models to observed  
14 subsidence from backstripping studies on sedimentary sections from wells in the basin  
15 interior. This results in a best-fit scenario with a 50-km thick initial plume head with a  
16 temperature of 1500 °C situated 50 km below the surface, and an initial regional crustal  
17 thickness of 34 km, in agreement with published values. Backstripping and modeling  
18 results agree very well, including a 60-90 Myr delay between the rifting phase and the  
19 first regional subsidence below sea level. Regional subsidence patterns indicate that the  
20 plume head was present across a minimum area of ~2.5 million km<sup>2</sup>. These results re-  
21 emphasize the viability of a mantle plume scenario for the Siberian Traps, provide

22 important constraints on the dynamics of mantle plume heads and suggest a thermal  
23 control for the subsidence of the West Siberian Basin.

24 **Keywords:** plume head, Siberia, basin, subsidence.

25

## 26 INTRODUCTION

27 The West Siberian Basin (WSB) is one of the largest intra-continental rift basins  
28 in the world, with an area of roughly 3.5 million km<sup>2</sup>, including prolongations in to the  
29 Yenisey-Khatanga Trough and the Kara Sea (Fig. 1). The basin is associated with the  
30 Siberian Traps, which form the largest Phanerozoic continental flood basalt province.  
31 These events are commonly interpreted to be the result of the impact of a mantle plume  
32 head at the base of the Siberian lithosphere (e.g. Richards et al., 1989).

33 An important feature of the WSB is the regional delay, on the order of 60-90  
34 Myrs, in the onset of sedimentation after the initial rifting (Saunders et al., 2005). The  
35 cause of this delay has been inferred to be decay of uplift generated by the thermal effect  
36 of a mantle plume (Campbell and Griffiths, 1990; Saunders et al., 2005), but so far this  
37 hypothesis has not been quantified. The subsidence patterns within the WSB also present  
38 an ideal opportunity to examine the generic spatial extent of spreading plume material  
39 beneath lithosphere. Previously this has only been estimated from the areal extent of  
40 volcanism (d'Acremont et al., 2003) and numerical models of plume head spreading  
41 (Campbell, 2007). By comparing subsidence patterns predicted by 1-D conductive heat  
42 flow models with those from backstripping, this study provides 1) a quantitative  
43 explanation for the cause of the subsidence delay after initial rifting, 2) independent

44 estimates of the lateral extent of the Siberian mantle plume head beneath the lithosphere,  
45 and 3) new constraints on mantle plume head dynamics.

46

## 47 **GEOLOGICAL BACKGROUND**

48 At the end of the Permian (~250 Ma) the WSB underwent extension associated  
49 with eruption of the Siberian flood basalts (Reichow et al., 2009). Figure 1 shows the  
50 locations of the main rifts and the extent of the flood basalts. The flood basalts reach a  
51 maximum thickness of 3 km in the northwest of the Siberian Craton. An average  
52 thickness of 2 km is deduced by Braitenberg and Ebbing (2009) from gravity modelling.  
53 Most authors agree that the flood basalts in the WSB were erupted sub-aerially (Westphal  
54 et al., 1998; Saunders et al., 2005; Vyssotski et al., 2006; Saunders et al., 2007) and  
55 therefore it is likely that the basement hadn't started to subside at the time.

56 During the Triassic, sediment deposition continued within the rifts at a reduced  
57 rate, but there was no deposition (or at least preservation) outside the rifts. In areas  
58 adjacent to the major rifts, sedimentation began in the Early Jurassic (~200 Ma). The first  
59 basin wide transgression did not occur until the Callovian (~165 Ma) (Peterson and  
60 Clark, 1991; Vyssotski et al., 2006). This is visible in the backstripped subsidence curves  
61 from Saunders et al. (2005) (Fig. 2). Sedimentation throughout the rest of the Mesozoic  
62 and early Cenozoic was strongly influenced by changes in global sea level. There was  
63 little further tectonic activity within the basin after the rifting.

64 Vyssotski et al. (2006) reports the crustal thickness of the WSB varying from a  
65 minimum of 34 km within the rifts to ~44 km at its margins. The average thickness  
66 across the basin is ~38 km, which is significantly thinner than the Siberian craton to the

67 east or the Ural mountains to the west. The thickness of the lithosphere beneath the WSB  
68 is not certain. Artemieva and Mooney (2001) used heat flow data to model the  
69 geothermal gradient, and calculated a lithosphere thickness of ~ 125 km across the WSB.  
70 In comparison, Priestley and McKenzie (2006) used shear wave velocity gradients to  
71 calculate a thickness of ~180 km.

72 It is important to assess the viable range of possible temperatures, thicknesses and  
73 depths of a plume head impacting on the base of the WSB lithosphere. The temperature  
74 can be estimated from the composition of the erupted volcanics. Saunders et al. (2005)  
75 used trace element ratios to argue for a decrease in the depth of melting from > 100 km to  
76 100-50 km over the evolution of the flood basalts. We interpret this to show that the  
77 plume effectively thins the overlying lithosphere to ~50 km.

78 The thickness of a plume head spreading out beneath continental lithosphere was  
79 investigated by Nyblade and Sleep (2003) who calculated thickness in the order of 10s of  
80 km. They also calculate that a 40 km thick plume head with an excess temperature of 200  
81 °C will thin the lithosphere by 50 km. In contrast, Campbell's (2007) model of plumes  
82 originating at the core mantle boundary show that the plume head may have had a  
83 thickness of  $175 \pm 25$  km. Therefore this parameter is not well-constrained for any  
84 possible plume head, including the Siberian example.

85

## 86 **METHODOLOGY**

87 A 1-D forward thermal model was used to examine whether the cooling of a  
88 thermal anomaly generated by a plume head could cause the subsidence in the WSB.  
89 Conductive heat flow through the lithosphere and upper mantle and the associated

90 subsidence of the column are calculated numerically. An in-depth description of the  
91 model is found in Holt et al. (2010). Temperature  $T$  for each depth  $z$  is integrated over  
92 time  $t$  by combining Fourier's law for conductive heat flow with conservation of energy  
93 and a radiogenic heat production  $A$ :

$$94 \quad \frac{\partial T}{\partial t} = \frac{1}{C_p \rho} \left\{ \frac{\partial}{\partial z} \left( k \frac{\partial T}{\partial z} \right) \right\} + \frac{A}{C_p \rho} \quad (1).$$

95 Specific heat  $C_p$  is related to the rock type, while density  $\rho$  is dependent on both  
96 temperature and rock type (Holt et al., 2010). The resulting density profile is used to  
97 calculate the isostatic height of the column relative to sea level calibrated to a column of  
98 mid-ocean ridge material with 2.7 km of water overlying a 7 km basaltic-gabbroic crust  
99 above a peridotitic upper mantle. For negative surface heights we extend the top of the  
100 column to sea level with water. This allows comparison with water-loaded tectonic  
101 subsidence calculations from backstripping. Similarly to water loading, sediment loading  
102 is also calculated to compare the model to the observed Moho depths. The sedimentation  
103 rate is assumed to keep pace with the subsidence. Since the Moho depths are those  
104 observed today and not the initial conditions, the model was run to produce a final crustal  
105 thickness, including sediments deposited in the basin that matches the present-day crustal  
106 thicknesses.

107         The temperature at the top (0 °C) and bottom (1381 °C) of the model are fixed  
108 using a potential temperature at the surface of 1330 °C, an adiabatic temperature increase  
109 of 0.3 °C/km and a model depth of 170 km. The model is benchmarked against sea-floor  
110 spreading models (Parsons and Sclater, 1977; Stein and Stein, 1992) for heat flow and  
111 bathymetry.

112           The initial conditions of the model are set up to match our current knowledge of  
113 the WSB as closely as possible. The crust is composed of a layer of flood basalt at the  
114 surface above a granitic upper crust and a lower crust with a density corresponding to  
115 granulite and mafic intrusions related to the volcanics at the surface. The thickness of the  
116 crust is varied, as are the flood basalt thickness and the upper – lower crust ratio to model  
117 the changes across the WSB. The crust is underlain by mantle lithosphere down to the top  
118 of the plume head. The initial temperature profile is a linear gradient from the surface,  
119 and intersects the mantle adiabat at the top of the plume head. The (initially constant)  
120 temperature, thickness and position of the underlying plume head are varied. Below the  
121 plume head, the temperature follows the mantle adiabat. This results in the base of the  
122 lithosphere settling at ~ 150 km (using the 1200 °C definition of Stein and Stein (1992))  
123 after 250 Myrs, which is an intermediate value of the various estimates of present-day  
124 lithospheric thickness.

125

## 126 **THERMAL SUBSIDENCE CURVES**

127           Backstripped wells from Saunders et al. (2005) were used to test the models as  
128 they cover a broad range of locations within the WSB, with different crustal and  
129 sedimentary thicknesses (Fig. 1). The backstripping analysis showed earlier onset of  
130 sedimentation in the rifts, around 250 – 240 Ma, and a greater amount of subsidence than  
131 the wells from the wider basin, where the onset of sedimentation was between 200 and  
132 160 Ma (Fig. 2).

133           The backstripped wells are shown alongside the modeled subsidence in Fig.2.  
134 Best fits are obtained with a plume head from 50 km to 100 km depth, with a temperature

135 of 1500 °C. An initial crustal thickness of 34 km produces a subsidence curve that fits the  
136 wells outside the rifts (N, Sa, Sl, Su), giving a final crustal thickness including the  
137 sediments of 37 km. This is equivalent to present crustal thicknesses across the WSB,  
138 outside of the main rifts (Vyssotski et al., 2006). Subsidence curves for wells within the  
139 rifts are successfully modeled by an initial crustal thickness of 30 km (Fig. 2). Changes in  
140 only the initial crustal thickness are sufficient to fit subsidence patterns in the rifts and in  
141 the wider basin. Well data from outside the rifts is representative of more regional  
142 subsidence patterns. The 3 km contour of sediment thickness from Vyssotski et al. (2006)  
143 is a proxy for regional subsidence on the scale described above, and implies that the  
144 plume head lay under this area of over 2.5 million km<sup>2</sup>, with little variation in depth to  
145 the top of the plume head.

146         Sensitivities of model parameters are shown in Fig. 3. In each case one parameter  
147 is varied compared to a standard set up (Fig 3a). Results are very sensitive to crustal  
148 thicknesses (Fig. 3b); a 46 km thick crust never subsides below sea level so is unlikely to  
149 form a basin, whereas a 38 km thick crust starts with an elevation of 1400 m, which then  
150 subsides, dropping below sea level after 88 Myrs. For a crustal thickness of 34 km, the  
151 initial elevation is 360 m and the model drops below sea level after 14 Myrs. The likely  
152 variation in the flood basalt thickness in the WSB has a much smaller effect on the  
153 subsidence of the basin than the crustal thickness.

154         Plume temperatures were varied between 1400 – 1600 °C to cover the range of  
155 plausible temperatures following melting and thinning of the lithosphere (Fig.3c). Results  
156 reveal that a hotter plume results in more initial uplift and increases the length of time  
157 before a basin begins to form. However, plume temperature has only a relatively minor

158 influence. Furthermore, for all model runs the final temperature profile, and therefore the  
159 final subsidence, is the same.

160 To test the effect of the depth of the plume the model was run for a 50 km thick  
161 plume head situated various depths. The effect of plume head thickness was also tested.  
162 Fig. 3d shows that where the plume reaches a depth of 50 km the model starts  
163 significantly above sea-level regardless of its thickness. For a 120 km thick plume the  
164 initial elevation is 1700 m whereas a 50 km thick plume has an initial elevation of 1400  
165 m and the onset of sedimentation is hastened. There is little difference when compared to  
166 varying the depth of the plume. If a 50 km thick plume begins at 100 km depth then its  
167 initial elevation is 350 m above sea level, whereas if the plume is 20 km deeper then the  
168 initial elevation of the plume is 250 m below sea level. The results illustrate that the  
169 subsidence curve is much more sensitive to the depth of the plume head than the  
170 thickness of the plume head. This is because the temperature contrast of the plume with  
171 the normal geotherm is greater at shallower depth, which will cause a greater reduction in  
172 the density of the material and therefore more initial uplift. Variations in radioactive heat  
173 production were previously shown to have little effect on either the total subsidence  
174 or the shape of the subsidence curve (Holt et al., 2010), and therefore are not discussed in  
175 this study.

176

## 177 **DISCUSSION**

178 Uplift has been suggested in conjunction with the eruption of a number of other  
179 large igneous provinces (LIP's) including the Emeishan traps, the Deccan traps, the North  
180 Atlantic LIP and Yellowstone (Saunders et al., 2007). Our modeling shows that if the



181 lithosphere is significantly thinned or heated, then isostasy alone will be enough to cause  
182 the uplift seen. This is in agreement with the recently proposed isostatic cause for the  
183 abnormal elevation seen in the American Cordillera (Hyndman and Currie, 2011)  
184 although the reason for the temperature anomaly is markedly different in each case. We  
185 have not included dynamic uplift in our model as it is a transient effect only acting while  
186 the plume was beneath the basin. Whether a plume can thin lithosphere, as our results  
187 indicate, is matter of debate both in active plume such as Hawaii and in numerical  
188 models. Ribe and Christensen (1999) calculated that the majority of the Hawaiian swell  
189 could be accounted for by dynamic uplift with only minor thinning of the lithosphere to  
190 89 km. Likewise in the model of Nyblade and Sleep (2003) there is some lithospheric  
191 thinning, but it limited to the rheological boundary layer at the base of the lithosphere. In  
192 contrast Li et al., (2004) showed that seismic data indicates that the lithosphere beneath  
193 Hawaii is only 50-60 km thick. Similarly the model of d'Acremont et al., (2003) that  
194 focus on implementing a realistic crust and mantle lithosphere rheology shows that strain  
195 rate and stress weakening of the lithosphere enhances its erosion by a plume head. Our  
196 study provides another line of independent evidence supporting thinning of the  
197 lithosphere. Geochemical evidence from the North Atlantic LIP (Kerr, 1994) shows such  
198 thinning is associated with other flood basalt provinces. The areal extent that the  
199 lithosphere is thinned over will likely vary somewhat between LIP's as the volumes of  
200 flood basalts do. d'Acremont et al (2003) use the extent of flood basalts visible at the  
201 surface to estimate that the plume head thins the lithosphere over an area  $\sim 3$  million  $\text{km}^2$ .  
202 Our method, using the subsidence patterns to give an indication of this, is preferable as

203 flood basalts can flow large distances from where they are erupted whereas the  
204 subsidence is more directly linked to the state of the lithosphere beneath it.

205

## 206 **CONCLUSIONS**

207 Comparing thermal subsidence curves from numerical heat flow models with  
208 backstripping results illustrates that the West-Siberian Basin subsidence is well explained  
209 by a 1500 °C, 50-km-thick plume head, impinging on a overlying lithosphere that is  
210 ~50 km thick after plume head emplacement with a 30 km thick crust in the rifts and a 34  
211 km thick crust in the wider basin. The modeling predicts that the subsidence in the WSB  
212 is most sensitive to the crustal thickness within the basin and depth to the top of the  
213 plume head, and shows less sensitivity to (reasonable) variation in the temperature and  
214 thickness of the plume head and the thickness of the flood basalts. Thermal modeling  
215 results show an excellent fit to both the magnitude and timing of subsidence, within the  
216 rifts and the wider basin. We conclude that the flood basalts, rifting and subsequent basin  
217 formation associated with the West Siberian Traps are best explained by a plume head  
218 which spreads out beneath the entire basin, while eroding the lithosphere to ~50 km  
219 thickness, and covering an area of over 2.5 million km<sup>2</sup>. We propose that quantitative  
220 comparison between modeled and observed subsidence of continental flood basalt  
221 provinces is a fruitful way to provide tighter constraints on the volume, lateral extent, and  
222 thermal erosion effects of mantle plume heads.

223

## 224 **ACKNOWLEDGMENTS**

225 We thank Statoil for funding, and Hans Marten Bjørnseth for his and constructive  
226 discussions.

227

## 228 **REFERENCES CITED**

229 Allen, M.B., Anderson, L., Searle, R.C., and Buslov, M.M., 2006, Oblique rift geometry  
230 of the West Siberian Basin: tectonic setting for the Siberian flood basalts: *Journal*  
231 *of the Geological Society*, v. 163, p. 901-904.

232 Artemieva, I.M., and Mooney, W.D., 2001, Thermal thickness and evolution of  
233 Precambrian lithosphere: A global study: *Journal of Geophysical Research*, v. 106,  
234 p. 16387-16414.

235 Braitenberg, C., and Ebbing, J., 2009, New insights into the basement structure of the  
236 West Siberian Basin from forward and inverse modelling of GRACE satellite  
237 gravity data: *Journal of Geophysical Research*, v. 114, doi:10.1029/2008JB005799.

238 Campbell, I.H., 2007, Testing the plume theory: *Chemical Geology*, v. 241, p. 153-176.

239 Campbell, I.H., and Griffiths, R.W., 1990, Implications of mantle plume structure for the  
240 evolution of flood basalts: *Earth and Planetary Science Letters*, v. 99, p. 79-93.

241 d'Acremont, E., Leroy, S., and Burov, E.B., 2003, Numerical modelling of a mantle  
242 plume: the plume head-lithosphere interaction in the formation of an oceanic large  
243 igneous province: *Earth and Planetary Science Letters*, v. 206, p. 379-396.

244 Holt, P.J., Allen, M.B., van Hunen, J., and Bjørnseth, H.M., 2010, Lithospheric cooling  
245 as a basin forming mechanism within accretionary crust: *Tectonophysics*, v. 495, p.  
246 184-194.

247 Hyndman, R.D., and Currie, C.A., 2011, Why is the North American Cordillera high?  
248 Hot backarcs, thermal isostasy and mountain belts: *Geology*, v. 39, no 8, p. 783-  
249 786.

250 Kerr, A.C., 1994, Lithospheric thinning during the evolution of continental large igneous  
251 provinces: A case study from the North Atlantic Tertiary province: *Geology*, v. 22,  
252 p.1027-1030.

253 Li, X., Kind, R., Yuan, X., Wölbern, I., and Hanka, W., 2004, Rejuvenation of the  
254 lithosphere by the Hawaiian plume: *Nature*, v. 427, p. 827-829.

255 Nyblade, A.A., and Sleep, N.H., 2003, Long lasting epeirogenic uplift from mantle  
256 plumes and the origin of the Southern African Plateau: *Geochemistry Geophysics*  
257 *Geosystems*, v. 4, p. 1-29.

258 Parsons, B., and Sclater, J.G., 1977, An analysis of the variation of the ocean floor  
259 bathymetry and heat flow with age: *Journal of Geophysical Research*, v. 108, p.  
260 803-827.

261 Peterson, J.A., and Clark, J.W., 1991, *Geology and hydrocarbon habitat of the West*  
262 *Siberian Basin*: Tulsa, Oklahoma, AAPG.

263 Priestley, K., and McKenzie, D., 2006, The thermal structure of the lithosphere from  
264 shear wave velocities: *Earth and Planetary Science Letters*, v. 244, p. 285-301.

265 Reichow, M.K., Pringle, M.S., Al'Mukhamedov, A.I., Allen, M.B., Andreichev, V.L.,  
266 Buslov, M.M., Davies, C.E., Fedoseev, G.S., Fitton, J.G., Inger, S., Medvedev,  
267 A.Y., Mitchell, C., Puchkov, V.N., Safonova, I.Y., Scott, R.A., and Saunders,  
268 A.D., 2009, The timing and extent of the eruption of the Siberian Traps large

269 igneous province: Implications for the end-Permian environmental crisis: Earth and  
270 Planetary Science Letters, v. 277, p. 9-20.

271 Ribe, N.M., and Christensen, U.R., 1999, The dynamical origin of the Hawaiian  
272 volcanism: Earth and Planetary Science Letter, v. 171, p. 517-531.

273 Richards, M.A., Duncan, R.A., Courtillot, V.E., 1989, Flood basalts and hot-spot tracks:  
274 plume heads and tails: Science, v. 246, 103– 107.

275 Saunders, A.D., England, R.W., Reichow, M.K., and White, R.V., 2005, A mantle plume  
276 origin for the Siberian traps: uplift and extension in the West Siberian Basin,  
277 Russia: Lithos, v. 79, p. 407-424.

278 Saunders, A.D., Jones, S.M., Morgan, L.A., Pierce, K.L., Widdowson, M., and Xu, Y.G.,  
279 2007, Regional uplift associated with continental large igneous provinces: The  
280 roles of mantle plumes and the lithosphere: Chemical Geology, v. 241, p. 282-318.

281 Stein, C.A., and Stein, S., 1992, A model for the global variation in oceanic depth and  
282 heat flow with lithospheric age: Nature, v. 359, p. 123-129.

283 Vyssotski, A.V., Vyssotski, V.N., and Nezhdanov, A.A., 2006, Evolution of the West  
284 Siberian Basin: Marine and Petroleum Geology, v. 23, p. 93-126.

285 Westphal, M., Gurevitch, E.L., Samsonov, B.V., Feinberg, H., and Pozzi, J.P., 1998,  
286 Magnetostratigraphy of the lower Triassic volcanics from deep drill SG6 in  
287 western Siberia: evidence for the long-lasting Permo-Triassic volcanic activity:  
288 Geophysical Journal International, v. 134, p. 254-266.

289

290

291

292 **Figure Captions**

293 Figure 1. Location of the West Siberian Basin (dashed line), the 3 km sedimentary thickness contour  
294 (dotted line) and the neighboring Siberian Craton (dot dash line). Red dots mark backstripped  
295 wells from Saunders et al. (2005). N=Novoport-130, S=SG-6, Sa=Samotlar-39, Sl=Salym-184,  
296 Su=Surgot-51, U=Urengoy-414. Modified from Allen et al. (2006).

297 Figure 2. Backstripped water-loaded subsidence from wells across the basin (Saunders et al., 2005) is  
298 compared to the subsidence produced by the forward model. The wells within the rifts are fitted  
299 best by a model with an initial 30 km thick crust. This does not fit the rift phase of SG-6 well  
300 because rifting is not included in the model, however it is a close fit to the thermal subsidence  
301 phase. Delayed onset in sedimentation seen from the wells outside the rifts is matched by a model  
302 with an initial crustal thickness of 34 km. In each of the above models the plume lies at 50-100 km  
303 depth and has an initial temperature of 1500 °C.

304 Figure 3. The sensitivity of the model to b) the thickness of the crust, and the variation in the flood basalt  
305 thickness, c) the temperature of the plume head and d) effect of the depth and thickness of the  
306 plume head. In each case only one parameter is varied while the rest are kept as a standard model,  
307 shown in a) and described in the text. It represents initial set up of the model and does not  
308 represent the best fitting model. The gray area on each graph encapsulates the backstripped  
309 subsidence curves shown in Fig. 2 from Saunders et al., (2005).

Figure 1  
[Click here to download high resolution image](#)

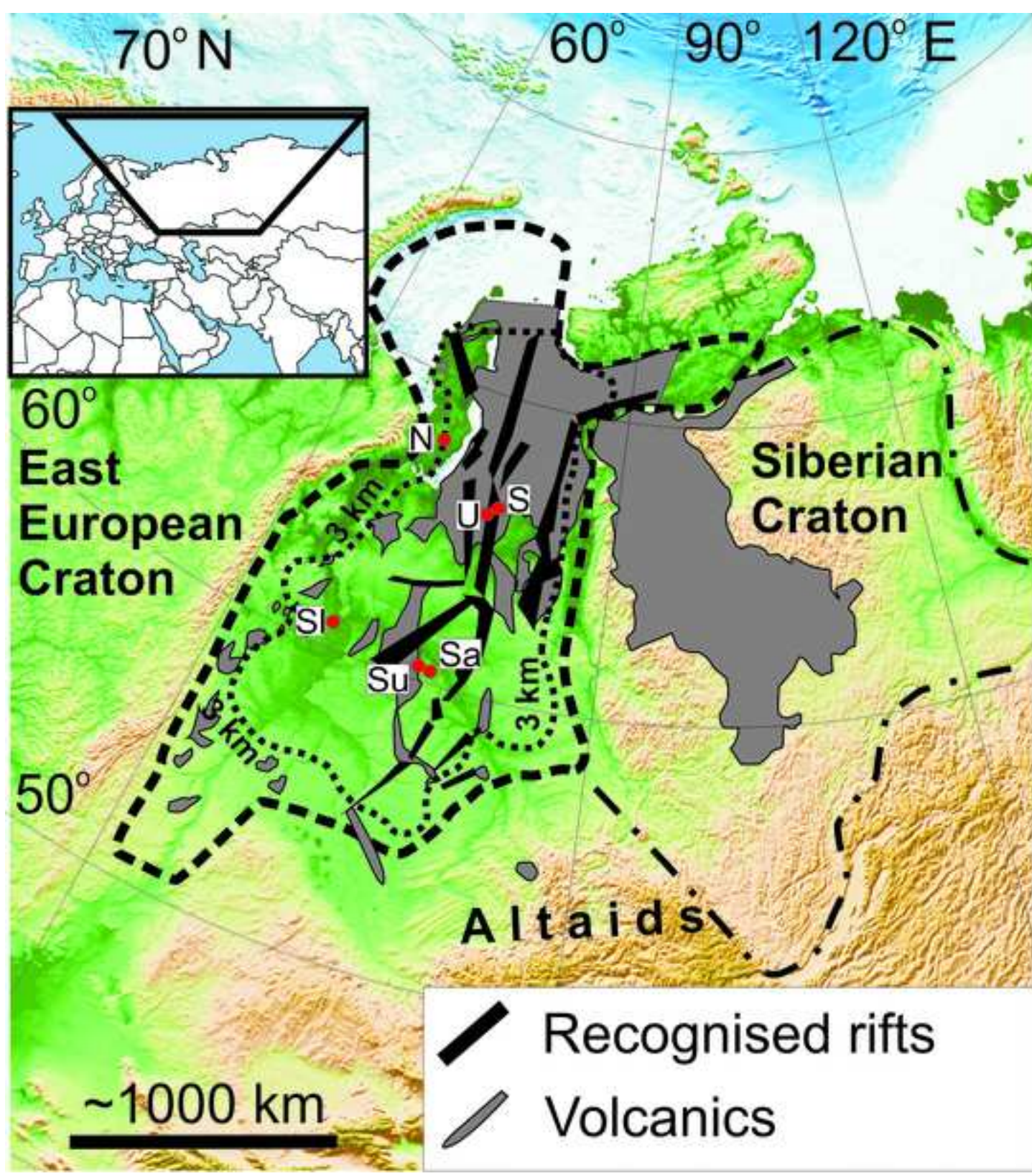


Figure 2  
[Click here to download high resolution image](#)

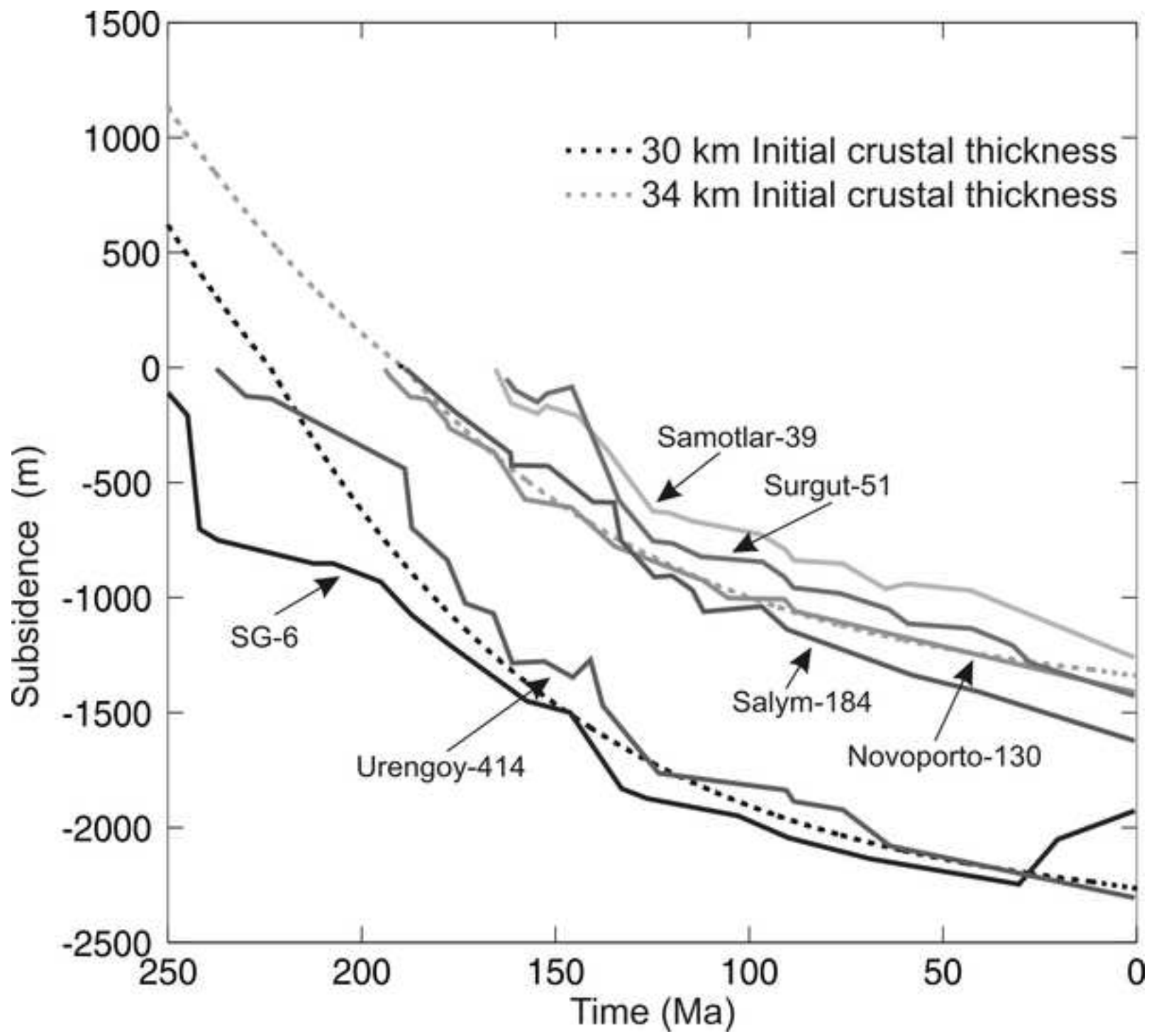




Figure 3

[Click here to download high resolution image](#)

